REVIEW OF SCIENTIFIC INSTRUMENTS 86, 063109 (2015)

Photoluminescence-based detection of particle contamination on extreme ultraviolet reticles

A. Gao,[1,a)] P. J. Rizo,[2] L. Scaccabarozzi,[2] C. J. Lee,[1] V. Banine,[2] and F. Bijkerk[1]
[1]*XUV Optics Group, MESA+ Institute for Nanotechnology, University of Twente, P.O. Box 217, 7500 AE Enschede, The Netherlands*
[2]*ASML, De Run 6501, 5504DR Veldhoven, The Netherlands*

(Received 2 October 2014; accepted 9 June 2015; published online 24 June 2015)

Here, we propose a comparison-free inspection technique to detect particle contamination on the reticle of extreme ultraviolet (EUV) lithography systems, based on the photoluminescence spectral characteristics of the contaminant particles and their elemental composition. We have analyzed the spectra from different particles found on reticles in EUV lithographic systems and have determined the minimum detectable particle size: 25 nm for organic particles and 100 nm for Al particles. Stainless steel coatings (50 nm thick and 50×50 μm^2 in area) exhibit detectable photoluminescence, and the estimated minimum detectable particle is 2 μm. © *2015 AIP Publishing LLC*. [http://dx.doi.org/10.1063/1.4922883]

I. INTRODUCTION

Optical lithography is one of the key technologies in semiconductor fabrication. Currently, the most advanced lithography systems use immersion techniques, based on 193 nm light. This technique is capable of printing features as small as 22 nm with a complex combination of techniques, such as double-patterning. Thus, the contribution of photolithography to the overall cost of integrated circuit fabrication is increasing.[1] Extreme ultraviolet lithography (EUVL), operating at a wavelength of 13.5 nm, is required to continuously reduce the feature sizes.[2] The dramatic decrease in wavelength will allow features smaller than 22 nm to be printed, using simpler patterning techniques.

EUV lithography systems require a clean environment, especially on the reticle, to ensure that the reticle pattern is printed with high fidelity. Although EUVL operates under vacuum conditions, contamination with small particles is unavoidable.[3] For example, particles can come from wearing of mechanical parts, dust during system assembly, manufacture debris. Particles can cause fatal defects on the final printed wafer, leading to a reduced yield of working chip devices. In current immersion-based lithography systems, DUV (deep ultraviolet) pellicles are used to protect reticles from particle contamination. Although new pellicle materials are being investigated, currently there are no pellicles available for EUVL systems.[4] Therefore, particles can be deposited onto the reticle, where they will be imaged on the wafer since they are in the object plane. Particles with a size comparable to the feature size on the wafer, e.g., 25 nm particles for the 22 nm chip process node, will result in defects on the exposed wafers. Particle contamination can be introduced to the reticle, either during handling outside of the lithography system or during exposure inside the system. The former has been largely mitigated by an advanced protection system, e.g., the dual-pod carrier system.[5] For the latter, reticle protection (pellicle), and/or, inspection, and cleaning are required.

Currently, the primary requirement for *in situ* inspection at the 22 nm process node is to detect 25 nm particles on a full size reticle (132×132 mm^2) within 1 h. The main difficulty with current inspection techniques, based on light scattering, is that the particle scatters light into a similar band of spatial frequencies as the features on the reticle, e.g., a particle would look like a contact hole when examining the scattering pattern. Hence, in an arbitrary reticle pattern, there is no way to detect the presence of a particle from the scattering pattern without comparison to a reference. Currently, inspection is done *ex situ* by imaging the surface at very high resolution (i.e., sub-100 nm pixels using 193 nm UV light) and comparing the image to a nominally identical location elsewhere on the wafer/reticle (die-to-die analysis) or to a calculated (or reference) image (die-to-database). However, it takes a few hours to inspect a whole reticle using this method, thereby, increasing the overall cost of semiconductor fabrication. Other inspection techniques, including E-beam inspection and actinic inspection, are under development.[6,7] Although they have shown detection of 30 nm or even smaller particles on patterned reticles, those techniques suffered from throughput and cost. Besides, due to their large volume, it is not yet possible to integrate them as an inspection module inside an EUVL system; thus, there is an additional risk that particles contaminate the reticle during the loading-unloading process of the lithography system.

Here, we propose a comparison-free and potentially *in situ* inspection method, using the intrinsic photoluminescence from contaminant particles to detect their presence on the reticle. The photoluminescent signal from the particle has a different wavelength from the excitation wavelength (laser), and the reticle will have little or no photoluminescence signal. Thus, the scattered light from the reticle can be filtered out, leaving only the photoluminescence signal from particles captured by the detector, as illustrated in Fig. 1. Since only the light signal from particles is captured, no comparison is

[a)]Electronic mail: a.gao@utwente.nl.

 © 2015 AIP Publishing LLC
This article is copyrighted as indicated in the article. Reuse of AIP content is subject to the terms at: http://scitationnew.aip.org/termsconditions. Downloaded to IP: 130.89.45.179 On: Tue, 27 Oct 2015 14:46:46

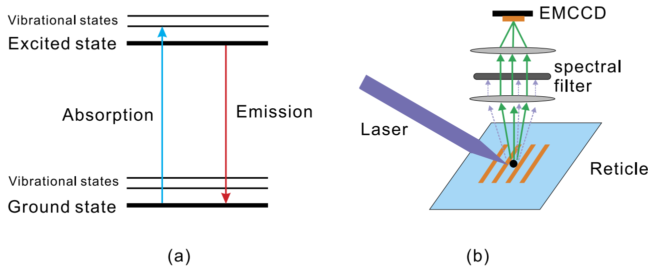

FIG. 1. (a) Principle of the photoluminescence process; (b) schematic view of the working principle for inspection based on the photoluminescence.

needed, which is an advantage over the techniques based on light scattering. This method also allows a fast scan with low resolution, followed by a high resolution scan, if required. The scan time of a whole reticle is determined by the resolution and the photoluminescence signal intensity from the contaminant particles. An additional advantage of this inspection method is that it is possible to identify the type of contaminant particles from their photoluminescence spectrum, thus allowing an appropriate cleaning mechanism to be chosen. In this paper, our primary experiments focus on determining the photoluminescent yield of typical particles found on reticles.

II. THEORY

The majority of contaminant particles on EUV reticles are stainless steel, aluminum, and organics (hydrocarbons); however, the contribution from each category varies substantially between reticles. And, although they are defined as stainless steel or aluminum particles, particles often contain a small fraction of other elements, e.g., Al particles may contain Mg and/or O. The different compounds have different potential sources of photoluminescence. Hydrocarbons are usually effective emitters under UV irradiation due to their complex electronic structures. Here, we do not distinguish between different organic molecules and simply refer to them as organic particles. Photoluminescence from metal particles is expected to be due to an oxidized outer shell, which occurs due to the presence of water in the residual gases of the EUV lithography system. The stainless steel particles in this study mainly contain Fe, Cr, and Ni. Cr naturally forms a passivation layer of oxide, which prevents surface erosion. Among the ionization states of Cr, Cr^{3+} has well known sharp emission line at 694 nm in a metal matrix composite.[8] NiO has also been reported to have emission lines at 312 nm and 400 nm under UV excitation.[9] For Al particles, it is also expected that the majority of the photoluminescence will originate from their oxide shell. Wide band emission in visible range has been reported in various studies of Al_2O_3 thin films.[10–14] Color centers in the oxide layer are the main source of photoluminescence. It is noted that small differences in composition of particles can lead to different photoluminescence yield. For example, some Al particles were found to contain a small amount of Mg. In addition, the photoluminescence spectrum from metallic particles depends on the oxidation process and, often, the presence of defects. As a result, differences between seemingly identical particles can lead to a different photoluminescence spectrum.

The quantum yield is one of the most important parameters of an emission center. The quantum yield is defined as the emitted photons relative to the number of absorbed photons. In this study, in order to include the excitation efficiency, we define the yield, $\boldsymbol{Q}$, as the emitted photons relative to the number of incident photons. The number of photons that results in detector counts can be estimated to be

$$C_{det} = \Phi_{inc}\pi R^2 A\eta_{emi}\eta_{col}\eta_{det}T, \quad (1)$$

where $\boldsymbol{C_{det}}$ is the counts at detector, Φ_{inc} is the incident photon flux, πR^2 is the particle area (with effective radius $\boldsymbol{R}$), $\boldsymbol{A}$ is the fraction of photons absorbed by the particle, η_{emi} is the emission efficiency of the particle, η_{col} is the collection efficiency, $\boldsymbol{T}$ is the transmission of system, and η_{det} is the quantum efficiency of detector. Note that Eq. (1) contains the assumption that the incident photons are absorbed within a certain depth, e.g., the thickness of oxide shell. $\boldsymbol{Q}$ can be, thus, derived by

$$Q = \frac{\Phi_{out}}{\Phi_{in}} = \frac{C_{det}}{\Phi_{inc}\pi R^2\eta_{col}\eta_{det}T} = A\eta_{emi}, \quad (2)$$

where Φ_{in} is the number of photons incident on the particle and Φ_{out} is the number of photons emitted by the particle. The number of photons or $\boldsymbol{Q}$ required for the particle to be detected depends on the photoluminescence intensity of the reticle (absorber, Ru capping layer, and Si/Mo multilayer). In this study, this is experimentally determined. The signal to noise ratio, i.e., photons emitted by the particles to the photons emitted by the reticle, is required to be larger than one to allow the particle to be detected. Here, we take a signal to noise ratio of 10 to eliminate almost all false positives during the inspection. A detailed calculation will be presented in Sec. V.

III. EXPERIMENTAL SETUP

A schematic drawing of the experimental setup used for investigation of photoluminescence-based detection of particles is shown in Fig. 2. There are three main building blocks: the laser systems (listed in Table I), sample stage, and collection system. By using three lasers, a wide spectral excitation range from the ultraviolet to the near IR is covered, which allows the optimal excitation wavelength to be found. The laser beam is focused using a custom made tunable beam shaping system. The beam shaping system focuses the laser beam into a rectangle with length of 4 mm and a width ranging from 100 μm to 1000 μm.

In the sample stage block, there is a sample holder that can handle standard 300 mm wafers, as well as smaller

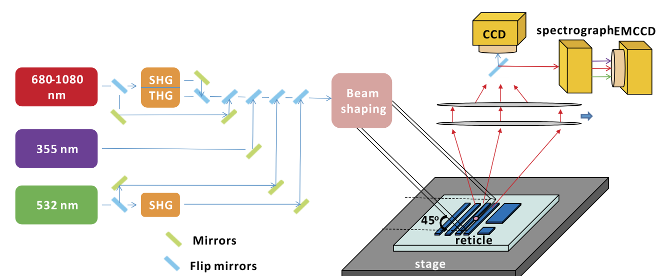

FIG. 2. Schematic view of the setup.

This article is copyrighted as indicated in the article. Reuse of AIP content is subject to the terms at: http://scitationnew.aip.org/termsconditions. Downloaded to IP: 130.89.45.179 On: Tue, 27 Oct 2015 14:46:46

TABLE I. Laser specifications.

Type	Wavelength range (nm)	Maximum average power
Continuous wave	532[a]	5 W
Continuous wave	266[a]	200 mW
ns pulsed	355	10 W
fs pulsed	680-1080	4 W
fs pulsed	340-540[b]	1 W
fs pulsed	230-360[b]	400 mW

[a]266 nm is the second harmonic of 532 nm.
[b]230-360 nm and 340-540 nm are the third and second harmonics of 680-1080 nm.

samples. The sample holder is placed on an x-y-z translation stage (AeroTech ES15800-1, AVSI125) with an absolute positional accuracy of 1 μm. To ensure that the sensitivity of the photoluminescence-based detection is accurately characterized, the stage positioning is correlated with a particle map, obtained from a phase contrast image (KLA Surfscan SP2). In this way, it is also possible to precisely locate target particles.

The collection block contains an objective with a NA = 0.13, a CCD camera (AVT Stingray F-080B) to obtain dark field images, and a spectrograph with two 300 lines/mm gratings, blazed for 350 and 500 nm, respectively (SOLAR Laser Systems, M266i), coupled to a high sensitivity EMCCD (electron multiplying charge coupled device) camera (Andor Technology, DU971P UVB, pixel size = 10 μm) to capture photoemission from the particle. The excitation wavelength was filtered out using two sets of filters (Semrock), which are detailed in Table II. The collection efficiency was calibrated using an HG-1 Mercury Argon Calibration Light Source and a Deuterium-Halogen Light Source (AvaLight-D(H)-S). Fig. 3 shows the collection efficiency curve from 200 to 1000 nm, including the collection optics with NA = 0.13, the loss through the lenses and mirrors, the transmission of the gratings in monochromator, and the quantum efficiency of EMCCD detector. The most effective collection range lies between 400 and 750 nm with the highest collection efficiency located at approximately 520 nm.

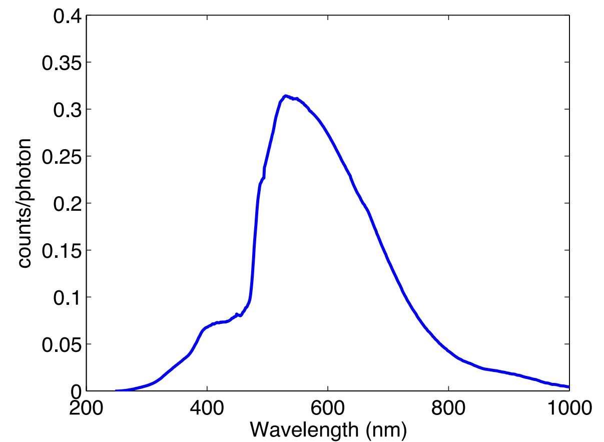

FIG. 3. System transmission.

IV. EXPERIMENT PROCEDURE

Particles were collected from the reticle in a real EUV lithography exposure process and then were transferred to a 300 mm wafer. The wafer was then scanned to identify the size and location of the particles by KLA Surfscan SP2. Certain particles were then analyzed using SEM-EDX (scanning electron microscope–energy dispersive X-ray) to obtain their chemical composition. A map with the information of particle size, location, and chemical composition was generated. The wafer containing the particles was then loaded into the photoluminescence setup. Dark field imaging was used to find chosen particles, using location data from the particle map. Finally, photoluminescence spectral measurements were obtained from the particle on the wafer.

V. RESULTS AND DISCUSSION

In Fig. 4, an Al particle is shown. It mainly contains O and Al with a very small amount of Mg. A weak photoluminescence spectrum (Fig. 4(b)) was obtained by using 266 nm excitation with an intensity of 76 W/cm^2. The bright horizontal streak in the center of the hyperspectral image in Fig. 4(b) is the photoluminescence signal from the Al particle during excitation. The strong emission lines from 550 nm that have no positional dependence are due to Raman scattering (from the second order of the diffraction grating) from the Si substrate, and the strong photoluminescence emission beyond 575 nm is also from Si substrate. We can see that the spectrum has a relatively low intensity and very broad spectral bandwidth (FWHM = 150 nm) with a peak at around 450 nm. To obtain optimum excitation, the photoluminescence excitation spectrum for Al particles was studied. In Fig. 5, we show a typical photoluminescence excitation spectrum, which has a peak at 420 nm. All other photoluminescence spectra for Al were taken using a laser excitation wavelength of 420 nm. All particle sizes in the following text refer to their diameter. As mentioned above, the Al particles may have different additives, which leads to different photoluminescence characteristics. In Fig. 6, we show two “Al” particles, particle 1 (diameter: 1.6 μm) contains Al, Mg, O, and C, while particle 2 (diameter: 490 nm) contains Al, O, and C (the majority element of these particles is Al, with the additives being only a very

TABLE II. Longpass filter specification.

Filter type	Cutoff wavelength (nm)	Transmission (%)	Filter type	Cutoff wavelength (nm)	Transmission (%)
LP02-266RU-25	266	≥ 90	FF02-409/LP-25	409	≥ 93
LP03-325RE-25	325	≥ 93	LP02-442RE-25	442	≥ 93
LP02-355RE-25	355	≥ 93	LP02-488RE-25	488	≥ 93
LP02-364RU-25	364	≥ 93	LP03-532RE-25	532	≥ 93

This article is copyrighted as indicated in the article. Reuse of AIP content is subject to the terms at: http://scitationnew.aip.org/termsconditions. Downloaded to IP: 130.89.45.179 On: Tue, 27 Oct 2015 14:46:46

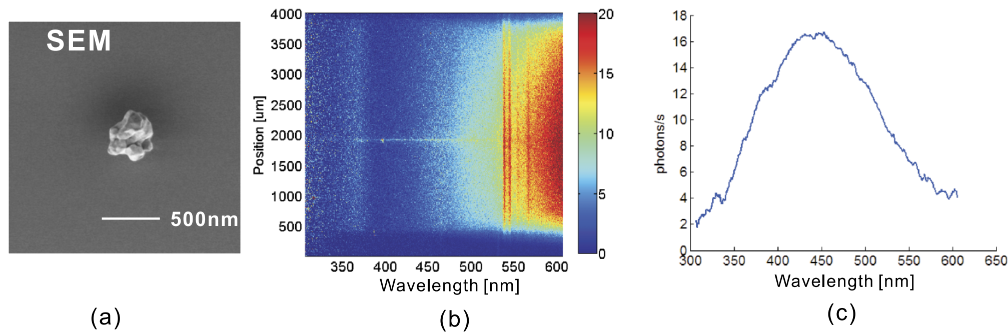

FIG. 4. Detection of an Al particle. (a) SEM image from the Al particle. (b) Hyper-spectral image of the photoluminescence signal from the Al particle. (c) The spectrum of the Al particle.

small fraction). However, these two particles show distinctive photoluminescence spectra: one spectrum peaks at around 500 nm, while the other peaks at 630 nm. This is expected because different dopants result in different color centers with different emission spectra. The difference will result in variations in $\boldsymbol{Q}$, which will be discussed later in this section.

An organic particle is shown in the SEM image in Fig. 7. It only contains C and O elements. Figure 7(b) is the hyperspectral image taken at an excitation wavelength of 420 nm with an intensity of 44 W/cm^2. The bright horizontal streak in the center of the hyperspectral image is the photoluminescence signal from the organic particle during excitation. The two strong emission lines that have no positional dependence are due to Raman scattering from the Si substrate. The broad photoluminescence spectrum, shown in Fig. 7(c), has a peak around 550 nm. All detected organic particles have similar spectra.

The photoluminescence signal from the same organic particle was also examined under 266 nm (11 W/cm^2) excitation. However, no signal was detected in this case. Furthermore, subsequent photoluminescent measurements at 420 nm (44 W/cm^2) revealed that the particle was no longer photoluminescent, indicating that the shorter wavelength excitation resulted in bleaching (see Fig. 8). To confirm this, a similar organic particle was exposed in a sequence of excitation wavelengths: 420 nm, 420 nm, 266 nm, and finally 420 nm. We found that there was a clear photoluminescence spectrum from the first and second exposures (420 nm excitation), but no signal in the following measurements with 266 and 420 nm excitations. The dark field images showed that the particles were not removed after exposure. These results indicate that organic particles are likely to be bleached by UV excitation.[15] No bleaching was observed for Al particles subjected to similar exposures.

Different sizes (from 100 nm to ∼μm) of stainless steel particles were also investigated. No photoluminescence signal was recorded. However, photoluminescence was observed on both a 50 nm thin stainless steel layer and 50 μm by 50 μm square pillar (Lab-grade, 50 nm thick). In Fig. 9, we show the photoluminescence signal of such stainless steel sample. Under excitation of 355 nm, the stainless steel exhibits a strong photoluminescence signal (similar spectra were observed for 420 nm and 266 nm excitations). Meanwhile, an array of 500 nm × 500 nm pillars (225 pillars, 50 nm high, fabricated at the same time and on the same sample substrate) showed no photoluminescence signal, which indicates that the photoluminescence from a small stainless steel particle is probably too weak to be detected by our setup. By comparing the surface areas of the pillar array and the pillar, the photoluminescence emission intensity from the 500 nm pillars was estimated to be 1 photon per second. If we extend the estimation to 25 nm particles, we expect 1 photon per 25 h.

The $\boldsymbol{Q}$ for all the inspected particles is summarized in the Fig. 10. The $\boldsymbol{Q}$ for different sizes of particles is calculated

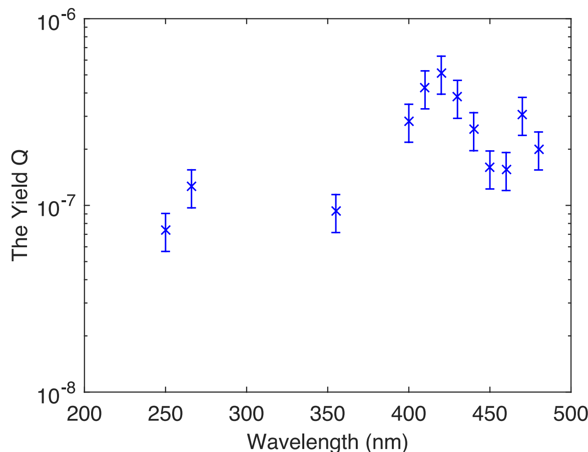

FIG. 5. The yield, $\boldsymbol{Q}$, of an Al particle as a function of excitation wavelength.

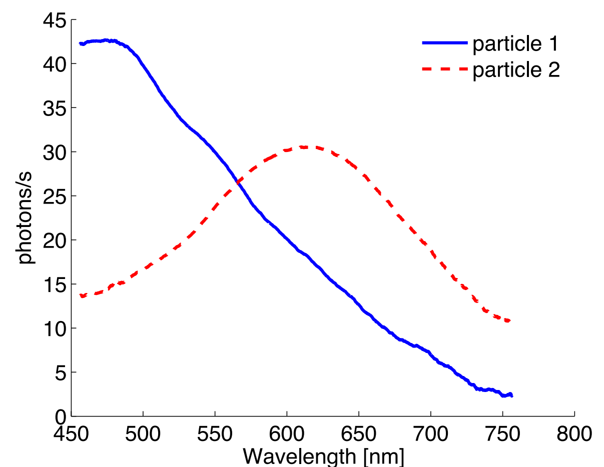

FIG. 6. Photoluminescence spectra for two types of "Al" particles with 420 nm excitation wavelength and excitation intensity of 44 W/cm^2.

This article is copyrighted as indicated in the article. Reuse of AIP content is subject to the terms at: http://scitationnew.aip.org/termsconditions. Downloaded to IP: 130.89.45.179 On: Tue, 27 Oct 2015 14:46:46

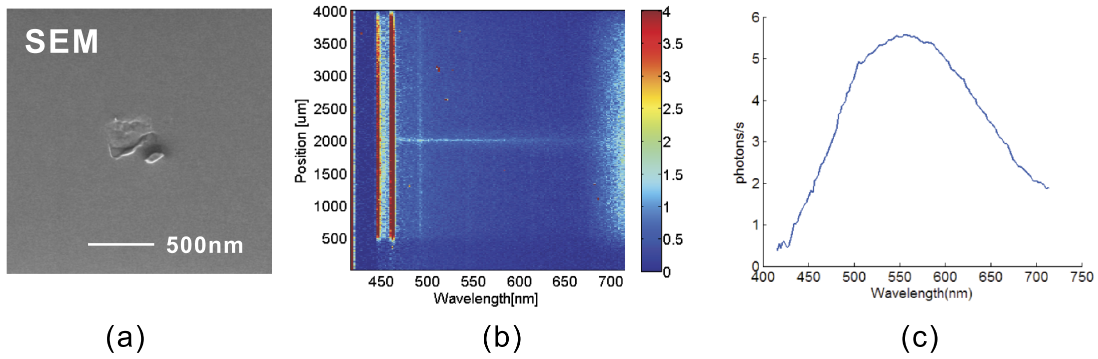

FIG. 7. Detection of an organic particle. (a) SEM image from the organic particle. (b) Hyper-spectral image of the organic photoluminescence signal. (c) The spectrum of the organic particle.

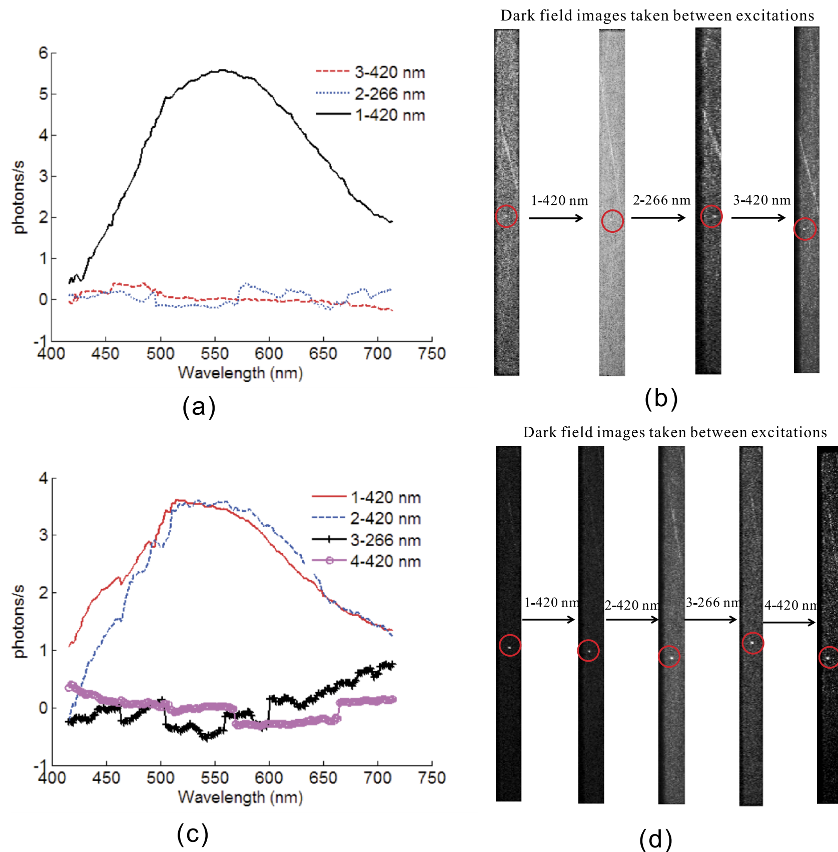

FIG. 8. Organic particle bleaching due to exposure to 266 nm excitation. (a) and (b) Organic particle was exposed in a sequence to 420 nm, 266 nm, and 420 nm excitations; (c) and (d) similar organic particle was exposed in a sequence to 420 nm, 420 nm, 266 nm, and 420 nm.

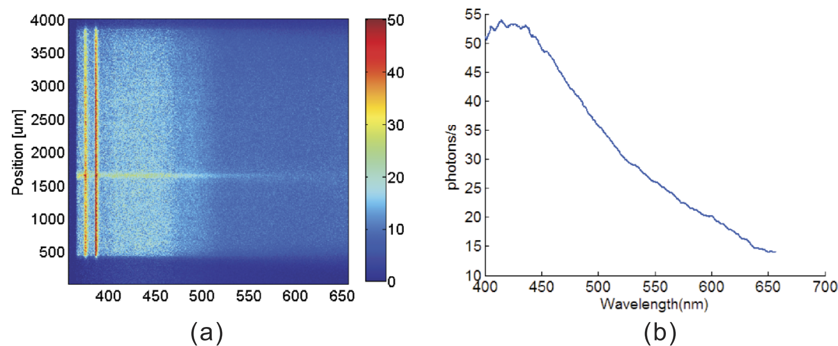

FIG. 9. Photoluminescence signal of stainless steel layer (area: 50 μm by 50 μm and thickness: 50 nm) with excitation at 355 nm and power density: 142 W/cm^2. (a) Hyperspectral image; (b) spectrum of the stainless steel.

This article is copyrighted as indicated in the article. Reuse of AIP content is subject to the terms at: http://scitationnew.aip.org/termsconditions. Downloaded to IP: 130.89.45.179 On: Tue, 27 Oct 2015 14:46:46

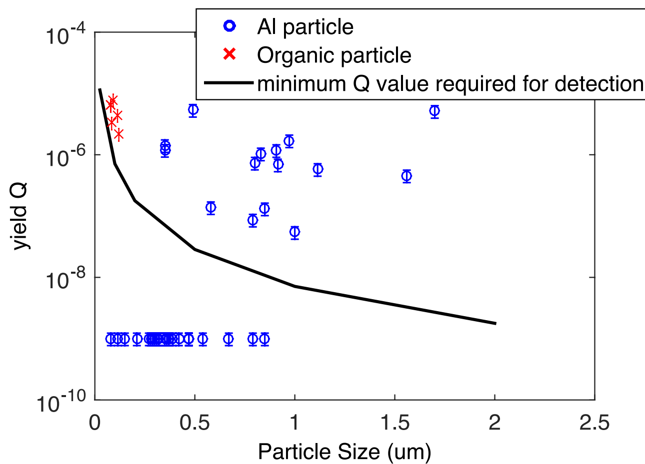

FIG. 10. Yield $\boldsymbol{Q}$ distribution for the inspected particles. All the particles were inspected using 420 nm excitation except that part of the detected Al particles were inspected with 266 nm excitation.

according to Eq. (2), based on the conditions that the incident laser intensity is 200 W/cm^2 (estimated damage threshold of the reticle) at 420 nm, and the photon counts for the system noise (including the photoluminescence signal from the reticle itself) are 20 photons/s. Considering the signal to noise ratio of 10, we can eliminate almost all the false positives during the inspection. Therefore, the signal from the particle reaching the detector needs to be 200 photons/s. The collection efficiency and the average system transmission are taken as 0.004 243 (based on NA = 0.13) and 30%, based on the measurements used to produce Fig. 3.

Fig. 10 shows that the $\boldsymbol{Q}$ for the organic particles, at least over the limited size range available, scales roughly with the inverse square of particle size, while for the Al particles, $\boldsymbol{Q}$ is very scattered. Note that all the organic particles that were targeted were also detected, while only about one third of the Al particles were detected. Based on the experimental data of the quantum yield-particle size relationship, we can estimate that it is possible to detect 25 nm organic particles (estimation is performed by putting the average measured $\boldsymbol{Q}$ value into the "minimum Q value required for detection" curve/formula and calculating the size). For the Al particles that emitted detectable photoluminescence, $\boldsymbol{Q}$ varied over 2 orders of magnitude. One possible explanation for the undetected Al particles is that the compositions for detected and undetected particles are slightly different, although they are all defined as Al particles. Different additives, such as C, Mg, and Fe, appear in the Al particles, i.e., corresponding to different Al alloys. This might lead to different types of color centers and, therefore, different yields.

The probability of detecting Al particles of 25 nm or smaller can be estimated by considering the color center density of the observed Al particles. The minimum number of color centers required to ensure that a particle is detected can be estimated from Fig. 10 and the literature values for color center properties. Although emission cross sections for color centers vary over a wide range, aluminum and Mg-doped aluminum oxide color centers are rather well studied. For these aluminum oxides, the emission cross section is known to be in the range 10^{-17}-10^{-18} cm^2.[16] The average excitation photon flux is Np 4.24×10^{20} cm^{-2}/s. Therefore, assuming that all absorbed excitation photons result in emitted photons,[16,17] the photon flux per color center ranges from 400 to 4000 photons per second. Using the instrument transfer function above, we estimate that a single color center generates 0.5 to 5 detected photons per second. Therefore, the detected particles must have at least 40 color centers, given the current experimental setup (requires 200 photons/s). Examining the particle sizes and their $\boldsymbol{Q}$, we note that the edge at which a particle may or may not exhibit photoluminescence is at a size of $\tilde{8}$00 nm, and no particles smaller than 350 nm were detected. Assuming an oxide layer thickness of $\tilde{5}$ nm, the observed color center density can be estimated between 4×10^{15}/cm^3 and 2×10^{16}/cm^3, assuming a total of 40 color centers in the particle. A particle with size of 25 nm will have 0.12–0.024

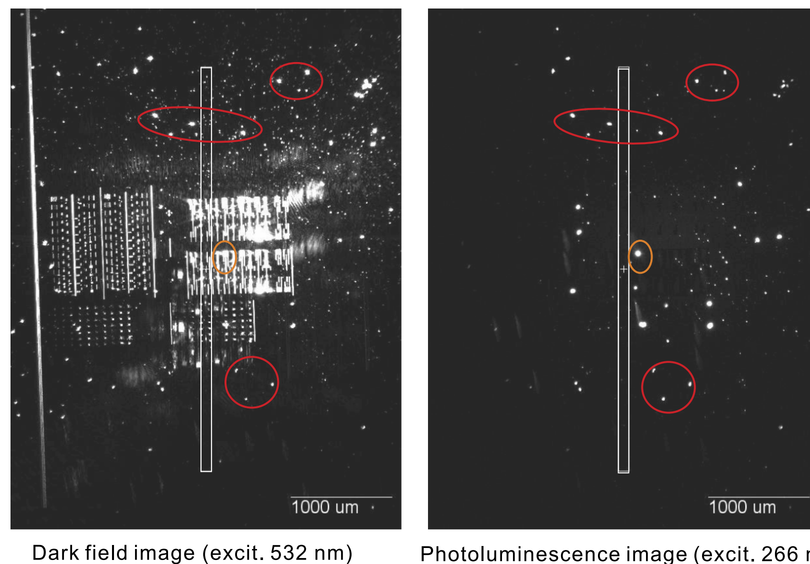

FIG. 11. Demonstration of the inspection concept with a real EUV reticle. Left picture: dark-field image of the reticle; right: photoluminescence image of the reticle, taken with 266 nm excitation and a 266 nm longpass filter.

This article is copyrighted as indicated in the article. Reuse of AIP content is subject to the terms at: http://scitationnew.aip.org/termsconditions. Downloaded to IP: 130.89.45.179 On: Tue, 27 Oct 2015 14:46:46

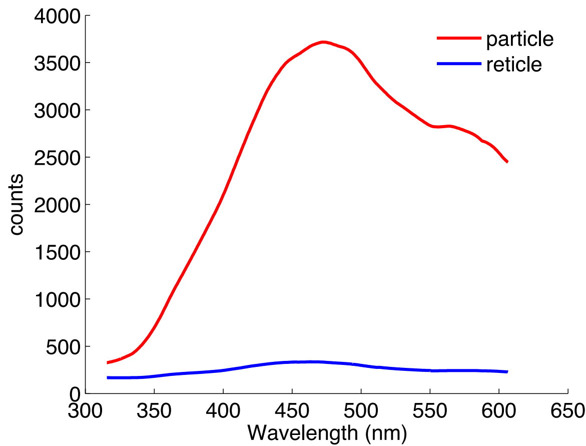

FIG. 12. The photoluminescence spectra comparison of a particle and reticle.

color centers; therefore, statistically less than one out of 10 Al particles will contain one color center. If we only require a signal to noise ratio slightly larger than 1, slightly more than 2 color centers per particle are required, which corresponds to a particle size of 60 nm. Fundamentally, if the setup is improved so that it can detect a single color center, i.e., remove most of the background noise signal, the minimum particle size that is detectable is 40 nm, based on our color center density estimation. However, the particle's metal core can strongly quench optical emission for polarizations that are parallel to the metal surface. It is, therefore, only possible for approximately half the color centers to emit efficiently in the direction of the collection optics (i.e., the minimum detectable size is about 80 nm). Returning to Fig. 10, smaller particles are undetectable because they have too few color centers. For larger particles, however, compositional differences lead to a wide range of color center densities, which enable some particles to be detected, while others remain undetectable. Using only the average value for Q and the minimum Q required for detection, it is estimated that the minimum detectable particle size for Al particles is found to be about 100 nm, which compares very well to the value derived from color center density estimates.

An in depth analysis of Q for stainless steel is not presented here. However, based on the data in Fig. 9, a Q of 1.6 $\times 10^{-9}$ is obtained, which will lead to a minimum detectable size of 2 μm. This value, however, is an over estimate, since the array of pillars has a combined (equivalent) size of 7.5 μm.

The method presented here has the potential to be integrated into an EUVL system for *in situ* inspection. In order to reduce the total inspection time for a full EUV reticle, a 2D image of the photoluminescent particle was made—that is, the integrated photoluminescence is recorded instead of a hyperspectral image (a hyperspectral image can still be taken to determine the type of the particle by switching the detector). As an example of a heavily polluted reticle, Fig. 11 shows the dark-field image (image of the scattering of the incident light) of the reticle and contaminant particles, and the photoluminescence image of the reticle and particles. Figure 11(b) shows that light scattering from the reticle is entirely removed by a long pass filter, leaving only the photoluminescence spectrum from the particles. Comparing the images in the unpatterned area (red circles), it shows that photoluminescent imaging does not detect all particles. Importantly, however, some particles within the patterned area are clearly visible (yellow circle). As can be seen from Figure 11(b), there is little-to-no photoluminescence signal from the reticle pattern, showing that the basic principle holds (see Fig. 12).

VI. CONCLUSION

An inspection setup for EUV reticles, based on element specific photoluminescence of contaminant particles, has been designed, built, and characterized. Critical contaminant particles from the reticle of an EUVL system, like organic (hydrocarbon), Al, and stainless steel particles, have been inspected. Organic particles with a size of 80 nm, i.e., the smallest available in this study, have been detected, while it is estimated that particles down to 25 nm are detectable. The smallest of the Al particles detected was 350 nm, while it is estimated that 100 nm particles can still be detected. Note that not all the Al particles larger than 350 nm can be detected. Stainless steel particles (100 nm to ~μm) were not detected, but stainless steel coatings did exhibit detectable photoluminescence. And based on experimental data, we estimate that particles larger than 2 μm can be detected. To ensure the reliable functioning of such a particle inspection tool, the fundamentals of photoluminescence from contaminant metal nanoparticles should be studied in more detail. For example, the particles on the EUV reticle will experience a short extreme UV exposure, in which the ionizing radiation is likely to induce color centers, increasing the possibility of detecting the smaller particles.[16] Finally, we note that, although the inspection method proposed here is for inspecting EUV reticles, it can be applied for detecting particle contamination on nano-imprint structures or templates.

ACKNOWLEDGMENTS

The authors would like to thank Mr. Goran Milinkovic, Mr. Luc Stevens, Mr. John de Kuster, and Dr. Lennino Cacace. This work is part of the research programme controlling photon and plasma induced processes at EUV optical surfaces (CP3E) of the Stichting voor Fundamenteel Onderzoek der Materie (FOM) with financial support from Carl Zeiss SMT and ASML, and the AgentschapNL through the EXEPT programme.

[1] P. Zimmerman, "Double patterning lithography: Double the trouble or double the fun?," SPIE Newsroom **20** (2009).
[2] C. Wagner and N. Harned, "Euv lithography: Lithography gets extreme," Nat. Photonics **4**, 24–26 (2010).
[3] T. E. Madey, N. S. Faradzhev, B. V. Yakshinskiy, and N. Edwards, "Surface phenomena related to mirror degradation in extreme ultraviolet (EUV) lithography," Appl. Surf. Sci. **253**, 1691–1708 (2006).
[4] H. Meiling, N. Buzing, K. Cummings, N. Harned, B. Hultermans, R. de Jonge, B. Kessels, P. Kürz, S. Lok, M. Lowisch *et al.*, "Euvl system: Moving towards production," Proc. SPIE **7271**, 727102 (2009).
[5] M. Amemiya, K. Ota, T. Taguchi, T. Kamono, Y. Usui, T. Takikawa, and O. Suga, "Particle-free mask handling techniques and a dual-pod carrier," Proc. SPIE **6921**, 69213T (2008).

This article is copyrighted as indicated in the article. Reuse of AIP content is subject to the terms at: http://scitationnew.aip.org/termsconditions. Downloaded to IP: 130.89.45.179 On: Tue, 27 Oct 2015 14:46:46

[6]M. Naka, S. Yamaguchi, M. Kadowaki, T. Koike, T. Hirano, M. Itoh, Y. Yamazaki, K. Terao, M. Hatakeyama, K. Watanabe *et al.*, "Capability of model EBEYE M for EUV mask production," Proc. SPIE **8522**, 85220k (2012).
[7]K. Goldberg and I. Mochi, "Wavelength-specific reflections: A decade of extreme ultraviolet actinic mask inspection research," J. Vac. Sci. Technol., B **28**, C6E1–C6E10 (2010).
[8]T. H. Maiman, R. Hoskins, I. d'Haenens, C. Asawa, and V. Evtuhov, "Stimulated optical emission in fluorescent solids. II. Spectroscopy and stimulated emission in ruby," Phys. Rev. **123**, 1151 (1961).
[9]Y. Wang, C. Ma, X. Sun, and H. Li, "Preparation and photoluminescence properties of organic–inorganic nanocomposite with a mesolamellar nickel oxide," Microporous Mesoporous Mater. **71**, 99–102 (2004).
[10]D. Liu, S. Clark, and J. Robertson, "Oxygen vacancy levels and electron transport in Al_2O_3," Appl. Phys. Lett. **96**, 032905 (2010).
[11]L. Brock, K. Mishra, M. Raukas, W. P. Lapatovich, and G. C. Wei, "Color centers in magnesium doped polycrystalline alumina," in *MRS Proceedings* (Cambridge University Press, 2001), Vol. 667, pp. G7–1.
[12]T. Perevalov, O. Tereshenko, V. Gritsenko, V. Pustovarov, A. Yelisseyev, C. Park, J. H. Han, and C. Lee, "Oxygen deficiency defects in amorphous Al_2O_3," J. Appl. Phys. **108**, 013501 (2010).
[13]J. Carrasco, J. R. Gomes, and F. Illas, "Theoretical study of bulk and surface oxygen and aluminum vacancies in α-Al_2O_3," Phys. Rev. B **69**, 064116 (2004).
[14]B. D. Evans and M. Stapelbroek, "Optical properties of the F^+ center in crystalline Al_2O_3," Phys. Rev. B **18**, 7089 (1978).
[15]M. V. Encinas, M. A. Rubio, and E. Lissi, "Quenching and photobleaching of excited polycyclic aromatic hydrocarbons by carbon tetrachloride and chloroform in micellar systems," Photochem. Photobiol. **37**, 125–130 (1983).
[16]V. V. Ter-Mikirtychev and T. Tsuboi, "Stable room-temperature tunable color center lasers and passive Q-switchers," Prog. Quantum Electron. **20**, 219–268 (1996).
[17]M. S. Akselrod, A. E. Akselrod, S. S. Orlov, S. Sanyal, and T. H. Underwood, "Fluorescent aluminum oxide crystals for volumetric optical data storage and imaging applications," J. Fluoresc. **13**, 503–511 (2003).

This article is copyrighted as indicated in the article. Reuse of AIP content is subject to the terms at: http://scitationnew.aip.org/termsconditions. Downloaded to IP: 130.89.45.179 On: Tue, 27 Oct 2015 14:46:46